NSRRC - Jo 4611 (2015)

Polymer Chemistry

PAPER

View Article Online
View Journal | View Issue

Published on 24 November 2014. Downloaded by National Tsing Hua University on 20/03/2015 01:16:04.

CrossMark click for updates

Cite this: *Polym. Chem.*, 2015, **6**, 1309

The backbone rigidity and its influence on the morphology and charge mobility of FBT based conjugated polymers†

Kuan-Yi Wu,[a] Chun-Chieh Chiu,[a] Wei-Tsung Chuang,[b] Chien-Lung Wang*[a] and Chain-Shu Hsu*[a]

Received 4th October 2014,
Accepted 23rd November 2014

DOI: 10.1039/c4py01361a

www.rsc.org/polymers

A series of three **PVTh$_4$FBT** polymers containing different alkyl side chain placement was synthesized. The thermochromic behaviors and DFT calculations indicated that the backbone coplanarity and rigidity of the **PVTh$_4$FBT** polymers can be effectively modulated by adjusting the side chain position and density. Higher ordered and better oriented edge-on lamellar packing was formed by **P1**, which possesses the most rigid backbone among the three polymers and pre-aggregates in the solution. **P1** also delivered the highest hole mobility (0.26 $cm^2 V^{-1} s^{-1}$) among the three analogues because its thin-film morphology is in favor of charge transport.

Introduction

Solution-processed organic field-effect transistors (OFETs) have attracted substantial research attention for their potential application as low-cost components in large-area flexible electronics.[1–3] Significant advances in molecular design and device physics have led to polymer-based OFETs with a charge mobility (μ) of over 1.0 $cm^2 V^{-1} s^{-1}$.

Based on the Marcus theory, low reorganization energies (λ_{reorg}s) and high degrees of intermolecular electronic coupling are conducive for conjugated molecules to reach high μ values.[4–9] By fusing the neighboring aromatic units, chemical rigidification inhibits inter-annular rotation. Thus, conjugated systems with multifused heteroarenes possess reduced λ_{reorg}s and a better coplanarity. Along with suitable lateral solubilizing side chains, effective intermolecular electronic coupling and a high μ have also been reported.[10,11] Recently, non-fused conjugated polymers also showed comparable and even higher μ values than their fused counterparts.[12–14] Without chemical rigidification, thiophene-based conjugated backbones are easily distorted through inter-annular rotation, as indicated by the low twist glass transition temperatures of poly(3-alkylthiophene)s.[15] The low energy barriers for the inter-annular rotation and the low conformational preferences of many non-fused donor–acceptor (D–A) backbones also lead to multiple possible spatial arrangements of the conjugated backbones and affect the polymer packing in the condensed phases.[16] Moreover, the backbone coplanarity and packing order of non-fused conjugated polymers are more sensitive to the bulkiness, chain lengths and attachment densities of the alkyl side chains.[17–20] To physically rigidify the non-fused backbones, the stability of the coplanar state, that is, the rigidity of the conjugated backbone, should be modulated.

The rigidity of the conjugated backbone can be affected by the main chain structure as well as the solubilizing side chains. 5,6-Difluorobenzo-2,1,3-thiadiazole (FBT) based D–A copolymers are conjugated polymers with high performances.[14,21–23] However, the ways of modulating the rigidity of FBT polymers and the influence of the backbone rigidity on the packing order and the charge mobility have not been carefully studied. Since, theoretically, the FBT unit is considered to be inefficient at locking the conformations,[16] the backbone properties of non-fused FBT polymers can be critical to the solid-state order and the OFET performances. Herein, a family of 5,6-difluorobenzo-2,1,3-thiadiazole-4,7-diyl (FBT)-bis-(bithienylene)vinylene **PVTh$_4$FBT** copolymers – **P1**, **P2**, and **P3** (Scheme 1) – was synthesized. All three polymers share the same backbone structure, but **P1** and **P2** are different in their side chain positions and **P3** has a higher side chain density than the other two. The influence of the vinylene group, along with the position and attached density of the side chains, on the backbone rigidity, solid-state morphology and OFET mobility was investigated. The results show that the backbone

[a]*Department of Applied Chemistry, National Chiao Tung University, 1001 Ta Hsueh Road, Hsin-Chu, 30010, Taiwan. E-mail: kclwang@nctu.edu.tw, cshsu@mail.nctu.edu.tw*

[b]*National Synchrotron Radiation Research Center, 101 Hsin-Ann Road, Hsinchu Science Park, Hsinchu, 300, Taiwan*

† Electronic supplementary information (ESI) available: The synthesis details, TGA measurements, DSC thermograms, cyclic voltammograms, AFM image, transistor data and the calculated input profile of **PTh$_4$VFBT** polymers. See DOI: 10.1039/c4py01361a

Published on 24 November 2014. Downloaded by National Tsing Hua University on 20/03/2015 01:16:04.

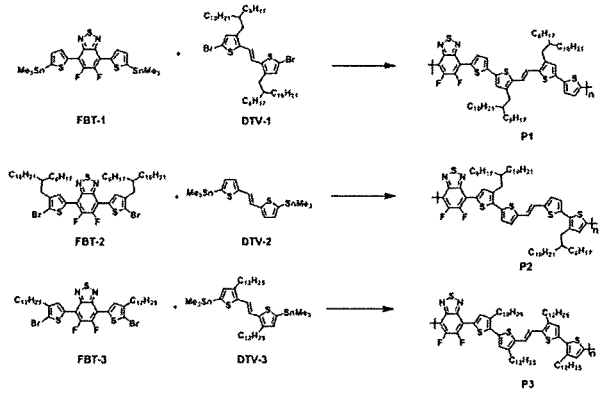

Scheme 1 Synthetic procedures of the **PVTh$_4$FBT** polymers. Reagents and conditions: tris(dibenzylideneacetone)dipalladium(0), tri(o-tolyl)-phosphine, chlorobenzene, 120 °C, 48 h.

rigidity of **PVTh$_4$FBT** can be effectively modulated by adjusting the side chain position and density. More importantly, the solid-state order and crystal orientations of the **PVTh$_4$FBT** polymers were affected by the backbone properties. The highest backbone rigidity of **P1** resulted in the most ordered and well-oriented edge-on lamellae on the substrate, which rendered **P1** with the highest μ_h among the three polymers.

Experimental section

General measurements and characterization

All chemicals were purchased from Aldrich or Acros and were used as-received unless otherwise specified. The synthesis and characterization of the FBT monomers, DTV monomers and polymers are summarized in the ESI.† FBT-1 was synthesized according to the literature.[14] ^{1}H and ^{13}C NMR spectra were recorded using a Varian 300 MHz instrument spectrometer. Molecular weights and polydispersity indices (PDI) of the polymers were determined by high temperature (120 °C) gel permeation chromatography (GPC) using a Viscotek module-350 system with polystyrene as the standard and 1,2,4-trichlorobenzene (TCB) as the eluent. Differential scanning calorimetry (DSC) was performed on a TA Q200 Instrument and thermogravimetric analysis (TGA) was performed on a Perkin Elmer Pyris under a nitrogen atmosphere at a heating rate of 10 °C min^{-1}. Absorption spectra were collected on an HP8453 UV-vis spectrophotometer. The electrochemical cyclic voltammetry (CV) was conducted on a CH Instruments Model 611D. A carbon glass coated with a thin polymer film was used as the working electrode and an Ag/Ag$^+$ electrode was used as the reference electrode, while 0.1 M tetrabutylammonium-hexafluorophosphate (Bu_4NPF_6) in acetonitrile was used as the electrolyte. CV curves were calibrated using ferrocene as the standard whose oxidation potential was set at −4.8 eV with respect to zero vacuum level. The E_{HOMO}s were derived from the equation $E_{HOMO} = -(E_{ox}^{onset} - E_{(ferrocene)}^{onset} + 4.8)$ eV. The E_{LUMO}s were derived from the equation $E_{LUMO} = -(E_{red}^{onset} - E_{(ferrocene)}^{onset} + 4.8)$ eV. A Veeco Diinnova atomic force microscope (AFM) in the tapping mode was used to characterize the surface morphology of the polymer thin films. The grazing incidence X-ray diffraction (GIXD) patterns of **PVTh$_4$FBT** polymers were recorded at the BL01C2 beamline of the National Synchrotron Radiation Research Center (NSRRC) in Taiwan. The ring energy of NSRRC was operated at 1.5 GeV with a typical current of 300 mA. The wavelength of the incident X-rays was 1.0332 Å (12.0 keV), delivered from the superconducting wavelength-shifting magnet, and an Si(111) double-crystal monochromator. The samples were placed horizontally on a sample stage. With an incident angle of 0.2°, GIXD was conducted and the pattern was collected with a detector system that included a CMOS flat panel X-ray detector, C9728DK. The scattering wave vector, defined as $q = 4\pi \sin\theta/\lambda$ (with 2θ being the scattering angle), was calibrated using silver behenate, sodalite, and silicon powders, respectively. The thin films used in the AFM and GIXD measurements were prepared according to the processes used in the OFET fabrication.

Computational details

Quantum-chemical calculations were performed with the Gaussian09 suite employing the B3LYP density functional in combination with the 6-311G(d,p) basis set. Geometry optimizations were performed with tight SCF and convergence criteria and an ultrafine integration grid applying the GEDIIS optimization algorithm. The energy minimized conformations of each polymer segment was confirmed by frequency analysis. The torsion potential energy surface was produced by scan of single-point energy calculations at the B3LYP/6-311G(d,p) level, and the dihedral angle θ_2 was stepped in 10° increments from the optimized geometry.

OFET fabrication

An n-type heavily doped Si wafer with an SiO_2 layer of 300 nm and a capacitance per unit area of 11 nF cm^{-2} was used as the gate electrode and the dielectric layer. Thin films (40–60 nm in thickness) of polymers were deposited on the octadecyltrichlorosilane (ODTS)-treated SiO_2/Si substrates by spin-coating ODCB solutions (2.5 mg mL^{-1} and 5 mg mL^{-1}) or TCB solutions (2.5 mg mL^{-1}) of the polymers. Then, the thin films were annealed at 200 °C under a nitrogen atmosphere for 30 min. The gold source and drain electrodes (30 nm in thickness) were deposited by vacuum evaporation on the organic layer through a shadow mask, affording a bottom-gate, top-contact device configuration. Electrical measurements of OFET devices were carried out at room temperature under nitrogen using a 4156C (Agilent Technologies). The field-effect mobility was calculated in the saturation regime using the equation $I_{DS} = (\mu WC_i/2L)(V_G - V_T)^2$, where I_{DS} is the drain–source current, μ is the field-effect mobility, W is the channel width (1 mm), L is the channel length (0.1 mm), C_i is the capacitance per unit area of the gate dielectric layer, and V_G is the gate voltage.

This journal is © The Royal Society of Chemistry 2015

Published on 24 November 2014. Downloaded by National Tsing Hua University on 20/03/2015 01:16:04.

Results and discussion

Synthesis and thermal analysis

The synthetic routes to the **PVTh$_4$FBT** polymers are depicted in Scheme 1. Pd-catalyzed Stille-coupling copolymerization of 5,6-difluoro-4,7-bis(5-(trimethylstannyl)-thiophen-2-yl)benzo[*c*]-[1,2,5]thiadiazole (**FBT-1**) and (*E*)-1,2-bis(5-bromo-3-(2-octyl dodecyl)thiophen-2-yl)ethene (**DTV-1**) afforded the formation of **P1** in 73% yield; copolymerization of 4,7-bis(5-bromo-4-(2-octyldodecyl)thiophen-2-yl)-5,6-difluoro-benzo[*c*][1,2,5]thiadiazole (**FBT-2**) and (*E*)-1,2-bis(5-(trimethylstannyl)thiophen-2-yl) ethene (**DTV-2**) resulted in the formation of **P2** in 63% yield; and copolymerization of 4,7-bis(5-bromo-4-dodecylthiophen-2-yl)-5,6-difluorobenzo[*c*][1,2,5] thiadiazole (**FBT-3**) and (*E*)-1,2-bis(3-dodecyl-5-(trimethylstannyl)thiophen-2-yl)ethene (**DTV-3**) resulted in the formation of **P3** in 39% yield. The molecular weights and polydispersity (PDI) of the polymers are M_n = 32.3 kDa (PDI = 2.8) for **P1**, M_n = 38.2 kDa (PDI = 2.1) for **P2**, M_n = 11.2 kDa (PDI = 1.5) for **P3**. The **PVTh$_4$FBT** polymers exhibited good thermal stability with 1% weight loss temperatures (T_ds) over 360 °C as measured by thermogravimetric analysis (Fig. S1†). The polymers were heated up to 300 °C to avoid thermal degradation in the differential scanning calorimetry (DSC) analysis (Fig. S2†). The melting temperatures (T_m) and the crystallization temperature of **P2** were observed at 262 °C and 232 °C, respectively, but no phase transition was found for **P1** and **P3** below 300 °C. Since the grazing-incidence X-ray diffraction (GIXD) measurements discussed below confirmed that **P1–P3** all form ordered solid-state phases, the T_ms of the ordered phases of **P1** and **P3** should be above the upper temperature limit of the DSC measurements (300 °C), and thus, the melting processes of the two polymers were not detected. The lower T_m of **P2** indicated that the bulky 2-octyldodecyl (OD) substituent at the 4′ position (see Fig. S3† for the number code) of the (*E*)-1,2-bis(2,2′-bithiophen-5-yl)ethene structural unit decreases the thermal stability of the crystalline state. Since the three polymers share the same backbone, the DSC results gave the first indication that the alkyl chain position affects the backbone rigidity and phase stability of the **PVTh$_4$FBT** polymers.

Optical and electrochemical properties

The optical behaviors of the polymers were investigated by ultraviolet-visible (UV-Vis) spectroscopy in dilute *o*-dichlorobenzene (ODCB) solutions and as thin films on glass. The characteristics of the UV-Vis spectrum of the **PVTh$_4$FBT** polymers are summarized in Table 1. As shown in Fig. 1, the absorption bands with λ_{max}s of about 450 nm can be attributed to a localized π–π^* transition. The λ_{max} of the photo-induced intramolecular charge transfer (ICT) absorptions of **P1** is 655 nm. Compared to the λ_{max} of **PTh$_4$FBT** (the polymer analogue without the vinylene structural unit) in our previous study,[22] the absorption of **P1** bathochromic shifts by 80 nm. Thus, the vinylene unit effectively increases the conjugation length of the polymer. Compared to the ICT band of **P1**, the hypsochromic shifts of the **P2** and **P3** absorptions (Table 1) suggest decreases in the effective conjugation lengths.[24] Since

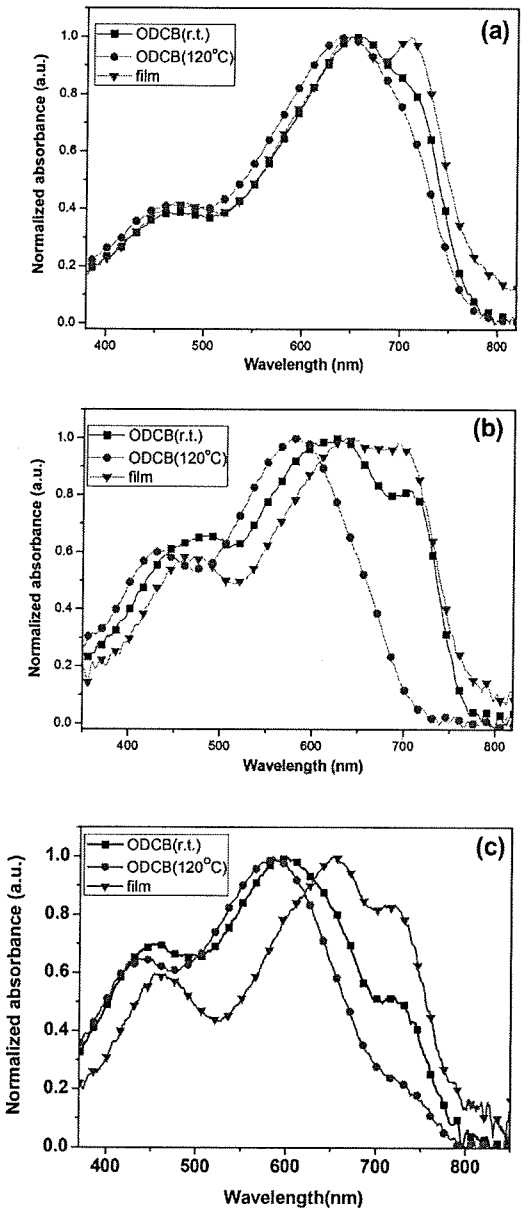

Fig. 1 Normalized UV-vis absorption spectra of (a) **P1**, (b) **P2** and (c) **P3** in an ODCB solution at room temperature (black square), at 120 °C (red circle), and in the thin-film state (green triangle).

Table 1 Optical and electrochemical properties of the **PVTh$_4$FBT** polymers

	λ_{max} (nm)				
Polymer	Solution	Film	$E_{g,opt}$ (eV)	E_{HOMO} (eV)	E_{LUMO} (eV)
P1	652, 704	652, 710	1.54	−5.23	−3.43
P2	620, 704	640, 706	1.57	−5.31	−3.02
P3	600, 706	655, 706	1.54	−5.27	−3.23

Published on 24 November 2014. Downloaded by National Tsing Hua University on 20/03/2015 01:16:04.

the three polymers share the same conjugated backbone, the disruption of the effective conjugation was attributed to the decreased backbone coplanarity caused by the OD side chains near the inter-thienyl bond (in the case of **P2**), and the increased side chain density (in the case of **P3**). Pre-aggregations of the copolymers in the ODCB solutions are evident at room temperature, since the 710 nm absorption shoulder observed in the thin films can also be found in the solutions. The weakest absorption shoulder of **P3** in solution indicates that the high side chain density may prevent effectively interchain interactions in the solution. Deduced from cyclic voltammetry measurements (Fig. S4†), the E_{HOMO}s and E_{LUMO}s of the polymers are also summarized in Table 1.

The backbone rigidities of the polymers were further evaluated by thermochromic experiments. At a solution temperature of 120 °C, the three polymers responded differently to the thermal disturbance. The increased solution temperature resulted in only a 2 nm hypsochromic shift to the ICT band of **P1**, but 37 nm and 15 nm hypsochromic shifts to those of **P2** and **P3**. Therefore, the effective conjugation and backbone coplanarity of **P1** are much more difficult to be thermally disturbed than the other two. The increased solution temperature also disaggregated the **PVTh$_4$FBT** polymers in the solution, as indicated by the decreased intensity of the 710 nm absorption bands. The photophysical behaviors of the **PVTh$_4$FBT** polymers thus reveal the strong influence of the side chain position and side chain density on the backbone properties of the polymers.

Theoretical calculations

Using Gaussian 09, density functional theory (DFT) calculations were performed on the simplified repeat units of the polymers at the B3LYP/6-311G(d,p) level.[25,26] The molecular segment of the **PVTh$_4$FBT** polymer shown in Fig. 2a was selected for the calculations to emphasize the influence of the alkyl side chains on the interannular dihedral angles (θ_1–θ_3) and the coplanarity of the backbone. To first evaluate the influence of the vinylene group, comparison of the **PVTh$_4$FBT** and **PTh$_4$FBT** backbones was made under conditions where alkyl side chains were excluded. As shown in Fig. 3, the smaller θ_2 and θ_3 angles of **PVTh$_4$FBT** indicate its better backbone coplanarity than that of **PTh$_4$FBT**. The improved coplanarity was attributed to the fact that the vinylene unit reduces the interannular steric hindrance.[27–31,32]

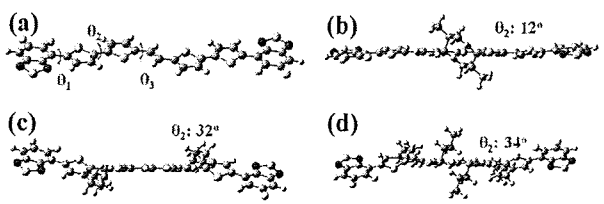

Fig. 2 (a) Illustration of the molecular segment of the PVTh$_4$FBT backbone and the interannular dihedral angles θ_1, θ_2, and θ_3. Side views of the optimized geometries of (b) **P1**, (c) **P2** and (d) **P3** at the B3LYP/6-311G(d,p) level of theory.

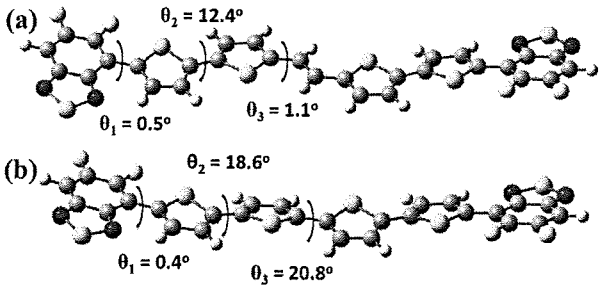

Fig. 3 The optimized geometries of (a) the PVTh$_4$FBT backbone and (b) the PTh$_4$FBT backbone at the B3LYP/6-311G(d,p) level of theory.

Table 2 Calculated dihedral angles in the optimized geometries of P1–P3

Polymer	θ_1 (°)	θ_2 (°)	θ_3 (°)
P1	0.5	12.0	2.2
P2	0.5	31.5	1.2
P3	0.4	34.1	3.0

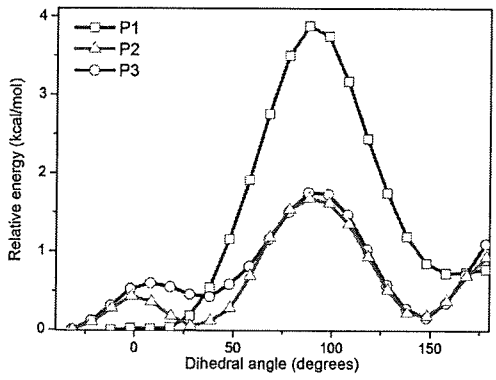

Fig. 4 Potential energy profiles of the PVTh$_4$FBT segments at the B3LYP/6-311G(d,p) level of theory.

The optimized conformations of the molecular segments of **P1**, **P2** and **P3** are shown in Fig. 2b–2d. The dihedral angles (θ_1–θ_3) in the optimized geometries of the three polymers are summarized in Table 2. The alkyl side chains degraded the backbone coplanarity as indicated by the increased interannular dihedral angles. The degree of interannular torsion depends on the alkyl side chain placement. As can be seen in the cases of **P1** and **P3**, the alkyl groups closer to the vinylene unit (4-position, see the number codes for the substituents in Fig. S3†) are less effective in distorting the backbone, while those closer to the inter-thienyl single bond (3′-position) evidently increased θ_2 from 12° to over 32°.

The backbone rigidity was further investigated by potential energy profiles of the molecular segments plotted in Fig. 4. In this figure, θ_2 = 0° corresponds to a fully planar conformation.

This journal is © The Royal Society of Chemistry 2015

Published on 24 November 2014. Downloaded by National Tsing Hua University on 20/03/2015 01:16:04.

The potential energy minima calculated for **P1**, **P2** and **P3** are located at θ_2 = 12°, 32°, and 34°, respectively, suggesting a gradual decrease in the backbone coplanarity. Upon rotation around the inter-thienyl bond, the potential energy increases, and attains a maximum E^* of 3.8 kcal mol^{-1} for **P1** and 1.62–1.75 kcal mol^{-1} for **P2** and **P3** at θ_2 = 90°. The increase of potential energy upon bond rotation indicates that torsion of the backbone is energetically unfavorable. The highest E^* of **P1** thus represents its highest backbone rigidity. The calculations agree with the results of the UV-Vis absorption experiments, where **P1** demonstrates the highest effective conjugation length and yet the lowest sensitivity to thermal agitation in the solution.

Grazing-incidence X-ray diffraction analysis

To analyze the solid-state order and chain orientation in the thin film, grazing-incidence X-ray diffraction (GIXD) measurements were performed on the thin films of the three polymers. The *d*-spacing and correlation length (L_{hkl}) deduced from the GIXD data are summarized in Table 3. In the GIXD patterns of the polymers shown in Fig. 5, the scattering from lamellar stacking ((*h*00) peaks) was observed along the q_z axis and the scattering from π–π stacking was observed along the q_{xy} axis. Thus, the edge-on lamellar orientation is preferable for the three polymers. However, the polymers did show different degrees of packing order and the orientational uniformity. High order peaks up to (400) were observed for the lamellar packing of **P1** and **P2**, while only up to (300) were found for the **P3** thin film. Moreover, as shown in Fig. 6, the broadness of the (100) peaks in the azimuthal scan increases from **P1** to **P2** to **P3**. Thus, the edge-on lamellar crystals of **P1** are more orderly oriented in the thin film than the other two. The lowest structural order of **P3** suggests that the increased side-chain density may deter the side-chain interdigitation and the registry between layers.[18] Consequently, the lamellar packing of **P3** is not only less ordered but also less oriented on the substrate. In contrast, as indicated by the thermochromic and calculation results, **P1** possesses a more planar and rigid backbone than the other two. The highly ordered and well-oriented edge-on lamellae of **P1** are thus related to its coplanar conformation in solution. The relationship is in line with Chen's study about Isoindigo-based polymers.[33]

Table 3 Summary of the polymer packing parameters in the thin films determined from the GIXD patterns

Polymer	Lamellar spacing (Å)	L_{100} (nm)	π–π spacing (Å)
P1	19.2	39	3.62
P2	19.7	28	3.62
P3	21.5	24	3.62

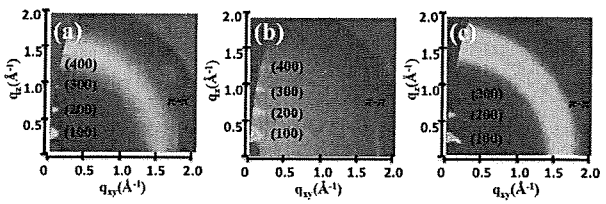

Fig. 5 GIXD patterns of (a) **P1**, (b) **P2**, and (c) **P3**.

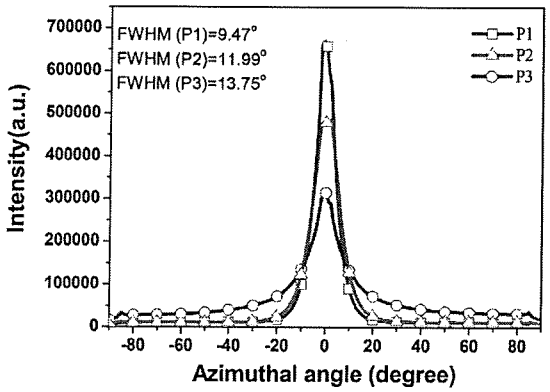

Fig. 6 The azimuthal-angle scans for the (100) peaks in the GIXD patterns of the **PVTh$_4$FBT** polymers. The inset shows the full width at half maximum (FWHM) of each azimuthal scan.

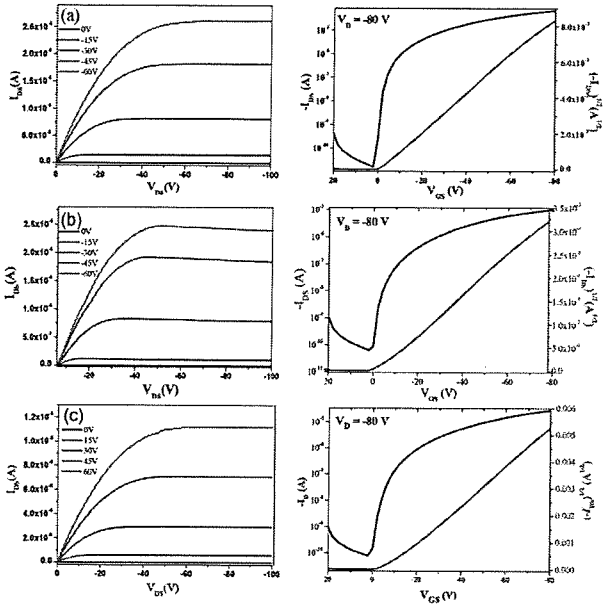

Fig. 7 Transfer (right) and output (left) characteristics of the OFET devices of (a) **P1**, (b) **P2** and (c) **P3**.

OFET performances

The charge transport properties of the **PVTh$_4$FBT** polymers were studied in OFET devices with a bottom-gate, top-contact configuration. The **PVTh$_4$FBT** polymers exhibited p-channel OFET characteristics, as shown in Fig. 7. The electrical characteristics of the devices including μ_h, threshold voltage (V_{th})

Published on 24 November 2014. Downloaded by National Tsing Hua University on 20/03/2015 01:16:04.

Table 4 OFET characteristics of the **PVTh$_4$FBT** polymers prepared from an ODCB solution at a concentration of 5 mg mL^{-1}

Polymer	$\mu_{h,avg}$ [a] ($\mu_{h,highest}$) (cm^2 V^{-1} s^{-1})	V_{th} [a] (V)	I_{on}/I_{off}
P1	0.22 (0.26)	−2.6	10^7
P2	0.027 (0.037)	−9.6	10^5
P3	0.086 (0.12)	−9.8	10^5–10^6

[a] Averaged value of over five devices.

Table 5 OFET characteristics of **P2** prepared from a reduced solution concentration (2.5 mg mL^{-1})

Solvent	$\mu_{h,avg}$ [a] ($\mu_{h,highest}$) (cm^2 V^{-1} s^{-1})	V_{th} [a] (V)	I_{on}/I_{off}
ODCB	0.089 (0.13)	−14.7	10^4–10^5
TCB	0.12 (0.17)	−16.7	10^3–10^5

[a] Averaged value of over five devices.

and the I_{on}/I_{off} ratio extracted from the figures are summarized in Table 4. **P1** delivered the highest μ_h (0.26 cm^2 V^{-1} s^{-1}) among the three polymers, which can be attributed to its most ordered and oriented solid-state structure. Unexpectedly, despite **P2** having better solid-state order than **P3**, it delivered the lowest averaged μ_h of 0.027 cm^2 V^{-1} s^{-1}. AFM revealed the surface topographies of the three polymer thin films (Fig. S5†). In Fig. S5b,† more grain boundaries were observed in **P2**. Because the presence of grain boundaries in the active layer is detrimental to charge mobility,[34–37] improving the thin-film morphology of **P2** was attempted. As shown in Fig. S6,† by reducing the concentration of **P2** solutions from 5.0 to 2.5 mg mL^{-1}, the film roughness (R_{RMS}) and the density of the grain boundary of the **P2** thin film can be significantly decreased. Consequently, the characteristics of the **P2** OFET devices (Fig. 7S†) were improved and the μ_h was increased to 0.089–0.12 cm^2 V^{-1} s^{-1} (Table 5) due to the improved morphology.

Conclusions

In this study, the vinylene group was introduced into a FBT based D–A polymer to physically planarize the conjugated backbone. The influence of alkyl chain position and density on the coplanarity and rigidity of the non-fused FBT based polymers was systematically compared in three **PVTh$_4$FBT** polymers. The thermochromic behaviors and DFT calculations indicated that the alkyl side chains close to the inter-thienyl bond and the high attached density increase the inter-thienyl dihedral angle, and decrease the energy barrier of the inter-annual bond rotation. Consequently, the backbones of **P2** and **P3** are less coplanar and less rigid than **P1**. The backbone coplanarity in solution further affects the packing order and crystal orientation of the polymers in the thin film. GIXD results showed that **P1** formed the most ordered and oriented edge-on lamellar packing among the three polymers. The highest μ_h of 0.26 cm^2 V^{-1} s^{-1} was delivered by **P1**, because its better solid-state order and suitable crystal orientation is conducive to the charge transfer in the OFET devices. Thus, the study revealed the critical role of the vinylene unit and the alkyl side chains in modulating the rigidity, packing order and OFET performances of **FBT** based polymers.

Acknowledgements

This work was supported by the National Science Council and "ATP" of the National Chiao Tung University and the Ministry of Education, Taiwan. The authors thank Prof. Keng S. Liang at Institute of Physics, Academia Sinica, Taiwan, Dr Hwo-Shuenn Sheu at beamline BL01C, and Dr U.-Ser Jeng at beamline BL23A of the National Synchrotron Radiation Research Center (NSRRC) in Taiwan for assistance with the XRD measurements.

Notes and references

1 A. C. Arias, J. D. MacKenize, I. McCulloch, J. Rivnay and A. Salleo, *Chem. Rev.*, 2010, **110**, 3–24.
2 J. Li, Y. Zhao, H. S. Tan, Y. Guo, C. A. Di, G. Yu, Y. Liu, M. Lin, S. H. Lim, Y. Zhou, H. Su and B. S. Ong, *Sci. Rep.*, 2012, **2**, 754.
3 H. Yan, Z. Chen, Y. Zheng, C. Newman, J. R. Quinn, F. Dotz, M. Kastler and A. Facchetti, *Nature*, 2009, **457**, 679–686.
4 Z. Chen, M. J. Lee, R. Shahid Ashraf, Y. Gu, S. Albert-Seifried, M. Meedom Nielsen, B. Schroeder, T. D. Anthopoulos, M. Heeney, I. McCulloch and H. Sirringhaus, *Adv. Mater.*, 2012, **24**, 647–652.
5 J. Fan, J. D. Yuen, W. Cui, J. Seifter, A. R. Mohebbi, M. Wang, H. Zhou, A. Heeger and F. Wudl, *Adv. Mater.*, 2012, **24**, 6164–6168.
6 I. Kang, T. K. An, J. A. Hong, H. J. Yun, R. Kim, D. S. Chung, C. E. Park, Y. H. Kim and S. K. Kwon, *Adv. Mater.*, 2013, **25**, 524–528.
7 T. Lei, J. H. Dou and J. Pei, *Adv. Mater.*, 2012, **24**, 6457–6461.
8 Y. Liu, H. Wang, H. Dong, J. Tan, W. Hu and X. Zhan, *Macromolecules*, 2012, **45**, 1296–1302.
9 Y. Liu, Q. Shi, L. Ma, H. Dong, J. Tan, W. Hu and X. Zhan, *J. Mater. Chem. C*, 2014, **2**, 9505–9511.
10 J. Mei, Y. Diao, A. L. Appleton, L. Fang and Z. Bao, *J. Am. Chem. Soc.*, 2013, **135**, 6724–6746.
11 I. Osaka, T. Abe, S. Shinamura and K. Takimiya, *J. Am. Chem. Soc.*, 2011, **133**, 6852–6860.
12 J. H. Kim, D. H. Lee, S. Yang da, D. U. Heo, K. H. Kim, J. Shin, H. J. Kim, K. Y. Baek, K. Lee, H. Baik, M. J. Cho and D. H. Choi, *Adv. Mater.*, 2013, **25**, 4102–4106.
13 H. Chen, Y. Guo, G. Yu, Y. Zhao, J. Zhang, D. Gao, H. Liu and Y. Liu, *Adv. Mater.*, 2012, **24**, 4618–4622.

This journal is © The Royal Society of Chemistry 2015

Published on 24 November 2014. Downloaded by National Tsing Hua University on 20/03/2015 01:16:04.

14 Z. Chen, P. Cai, J. Chen, X. Liu, L. Zhang, L. Lan, J. Peng, Y. Ma and Y. Cao, *Adv. Mater.*, 2014, **26**, 2586–2591.
15 K. Yazawa, Y. Inoue, T. Yamamoto and N. Asakawa, *Phys. Rev. B: Condens. Matter*, 2006, 74.
16 N. E. Jackson, B. M. Savoie, K. L. Kohlstedt, T. J. Marks, L. X. Chen and M. A. Ratner, *Macromolecules*, 2014, **47**, 987–992.
17 Z. Bao and A. J. Lovinger, *Chem. Mater.*, 1999, **11**, 2607–2612.
18 R. J. Kline, D. M. DeLongchamp, D. A. Fischer, E. K. Lin, L. J. Richter, M. L. Chabinyc, M. F. Toney, M. Heeney and I. McCulloch, *Macromolecules*, 2007, **40**, 7960–7965.
19 T. Prosa, M. Winokur and R. McCullough, *Macromolecules*, 1996, **29**, 3654–3656.
20 X. Zhang, L. J. Richter, D. M. DeLongchamp, R. J. Kline, M. R. Hammond, I. McCulloch, M. Heeney, R. S. Ashraf, J. N. Smith and T. D. Anthopoulos, *J. Am. Chem. Soc.*, 2011, **133**, 15073–15084.
21 H. Zhou, L. Yang, A. C. Stuart, S. C. Price, S. Liu and W. You, *Angew. Chem., Int. Ed.*, 2011, **123**, 3051–3054.
22 J. F. Jheng, Y. Y. Lai, J. S. Wu, Y. H. Chao, C. L. Wang and C. S. Hsu, *Adv. Mater.*, 2013, **25**, 2445–2451.
23 L. Yang, J. R. Tumbleston, H. Zhou, H. Ade and W. You, *Energy Environ. Sci.*, 2013, **6**, 316–326.
24 C. Yang, F. P. Orfino and S. Holdcroft, *Macromolecules*, 1996, **29**, 6510–6517.
25 F. C. Grozema, P. T. Van Duijnen, Y. A. Berlin, M. A. Ratner and L. D. Siebbeles, *J. Phys. Chem. B*, 2002, **106**, 7791–7795.
26 S. B. Darling and M. Sternberg, *J. Phys. Chem. B*, 2009, **113**, 6215–6218.
27 T. Lei, X. Xia, J. Y. Wang, C. J. Liu and J. Pei, *J. Am. Chem. Soc.*, 2014, **136**, 2135–2141.
28 N. B. Kolhe, A. Z. Ashar, K. S. Narayan and S. K. Asha, *Macromolecules*, 2014, **47**, 2296–2305.
29 J. C. Speros, H. Martinez, B. D. Paulsen, S. P. White, A. D. Bonifas, P. C. Goff, C. D. Frisbie and M. A. Hillmyer, *Macromolecules*, 2013, **46**, 5184–5194.
30 J. Shin, H. A. Um, D. H. Lee, T. W. Lee, M. J. Cho and D. H. Choi, *Polym. Chem.*, 2013, **4**, 5688.
31 T. Lei, J. H. Dou, X. Y. Cao, J. Y. Wang and J. Pei, *J. Am. Chem. Soc.*, 2013, **135**, 12168–12171.
32 J. Kim, B. Lim, K.-J. Baeg, Y.-Y. Noh, D. Khim, H.-G. Jeong, J.-M. Yun and D.-Y. Kim, *Chem. Mater.*, 2011, **23**, 4663–4665.
33 M. S. Chen, J. R. Niskala, D. A. Unruh, C. K. Chu, O. P. Lee and J. M. J. Fréchet, *Chem. Mater.*, 2013, **25**, 4088–4096.
34 H. Bronstein, J. M. Frost, A. Hadipour, Y. Kim, C. B. Nielsen, R. S. Ashraf, B. P. Rand, S. Watkins and I. McCulloch, *Chem. Mater.*, 2013, **25**, 277–285.
35 A. Salleo, R. J. Kline, D. M. DeLongchamp and M. L. Chabinyc, *Adv. Mater.*, 2010, **22**, 3812–3838.
36 B. Friedel, C. R. McNeill and N. C. Greenham, *Chem. Mater.*, 2010, **22**, 3389–3398.
37 R. Joseph Kline, M. D. McGehee and M. F. Toney, *Nat. Mater.*, 2006, **5**, 222–228.

This journal is © The Royal Society of Chemistry 2015